Decoupling the Capacity Fade Contributions of Polymer Electrolytes-Based High-Voltage Solid-State Batteries

Ji-young Ock[1,*], Sergiy Kalnaus[2], Michael J. Zachman[3], Andrew M. Ullman[1], Kyra D. Owensby[1,4], Oliver Long[1], Xi Chelsea Chen[1,*], Ritu Sahore[1,*]

[1]Oak Ridge National Laboratory, Chemical Sciences Division, Oak Ridge, TN 37831, USA

[2]Oak Ridge National Laboratory, Computational Science and Engineering Division, Oak Ridge, TN 37831, USA

[3]Oak Ridge National Laboratory, Center for Nanoscale Materials Sciences, Oak Ridge, TN 37831, USA

[4]The Bredesen Center for Interdisciplinary Research and Graduate Education, The University of Tennessee Knoxville, Knoxville, TN 37996, USA

***Corresponding authors:**

Jiyoung Ock: ockj@ornl.gov

Xi Chelsea Chen: chenx@ornl.gov

Ritu Sahore: sahorer@ornl.gov

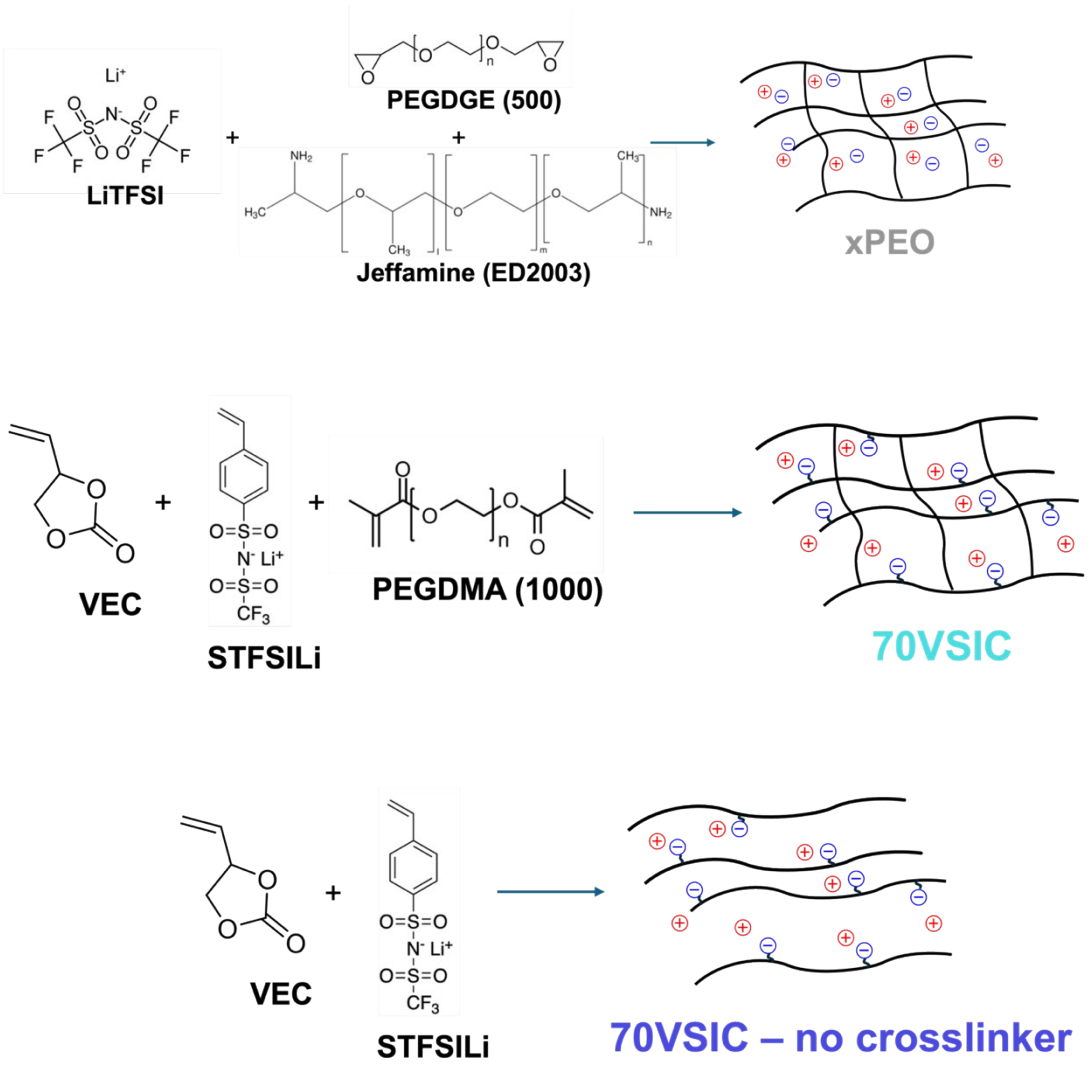

Figure S1. Chemical structures of the precursor compounds used for the fabrication of the three PEs.

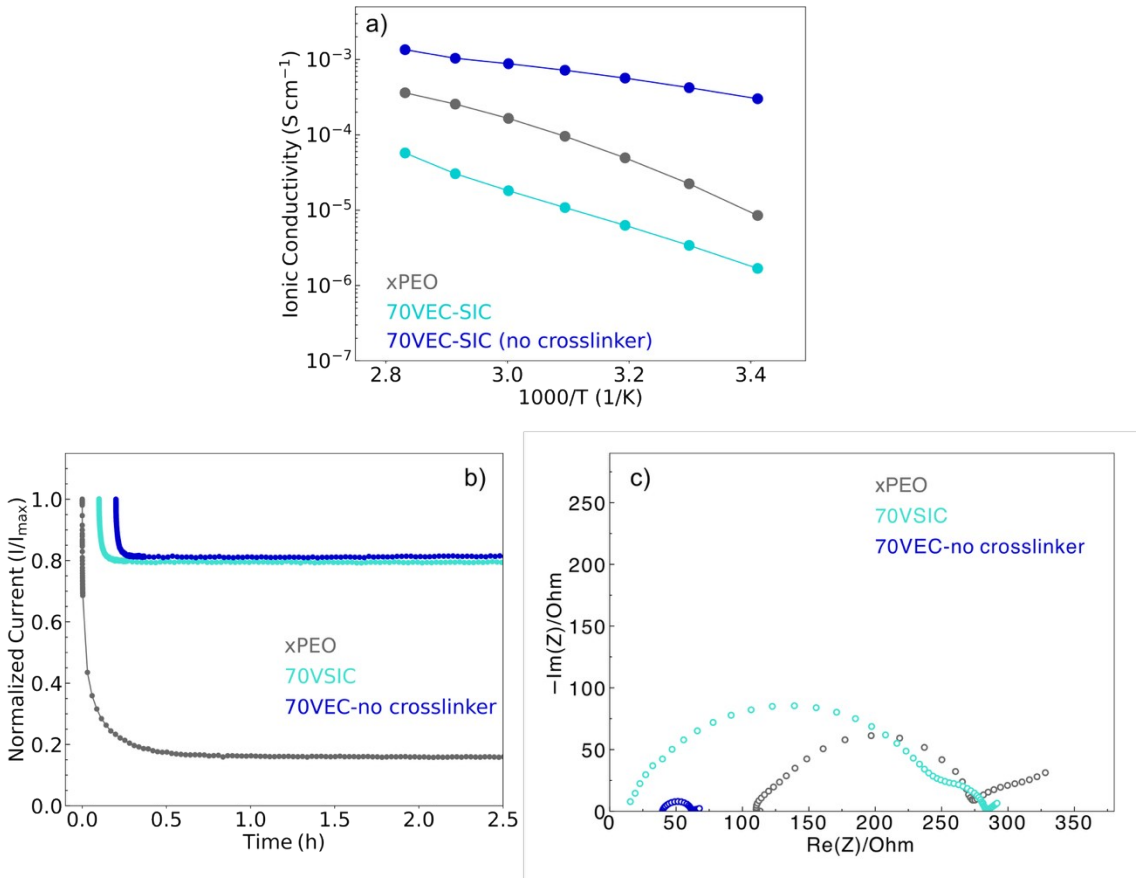

Figure S2. a) Arrhenius measurements of the ionic conductivity of the three polymer electrolytes utilized in this study. b) Normalized currents obtained for the three PEs during the chronoamperometry step of Bruce-Vincent method for Li^+ transference number measurement. The ionic conductivity and transference number of xPEO and 70VEC-SIC were reported in our previous publications. [1, 2] c) EIS of the 70VEC-SIC – no crosslinker Li||Li cell before the chronoamperometry step.

Table S1. Ion transport – related properties of the three polymer electrolytes utilized in this study, as measured via various experimental techniques as specified in the table.

	Temperature (K)	**Li Diffusivity (m^2/s) (NMR)**	**F diffusivity (m^2/s) (NMR)**	**Ionic Conductivity (S/cm) (SS bocking electrodes)**	**Li^+ Transference number (B-V method)**
xPEO	343	4.34×10^{-13}	9.99×10^{-12}	2.6×10^{-4}	0.05
70VEC-SIC	343	2.98×10^{-12}	-	3.1×10^{-5}	0.75
70VEC-SIC (no-crosslinker)	343	4.90×10^{-11}	1.20×10^{-11}	1.0×10^{-3}	0.75

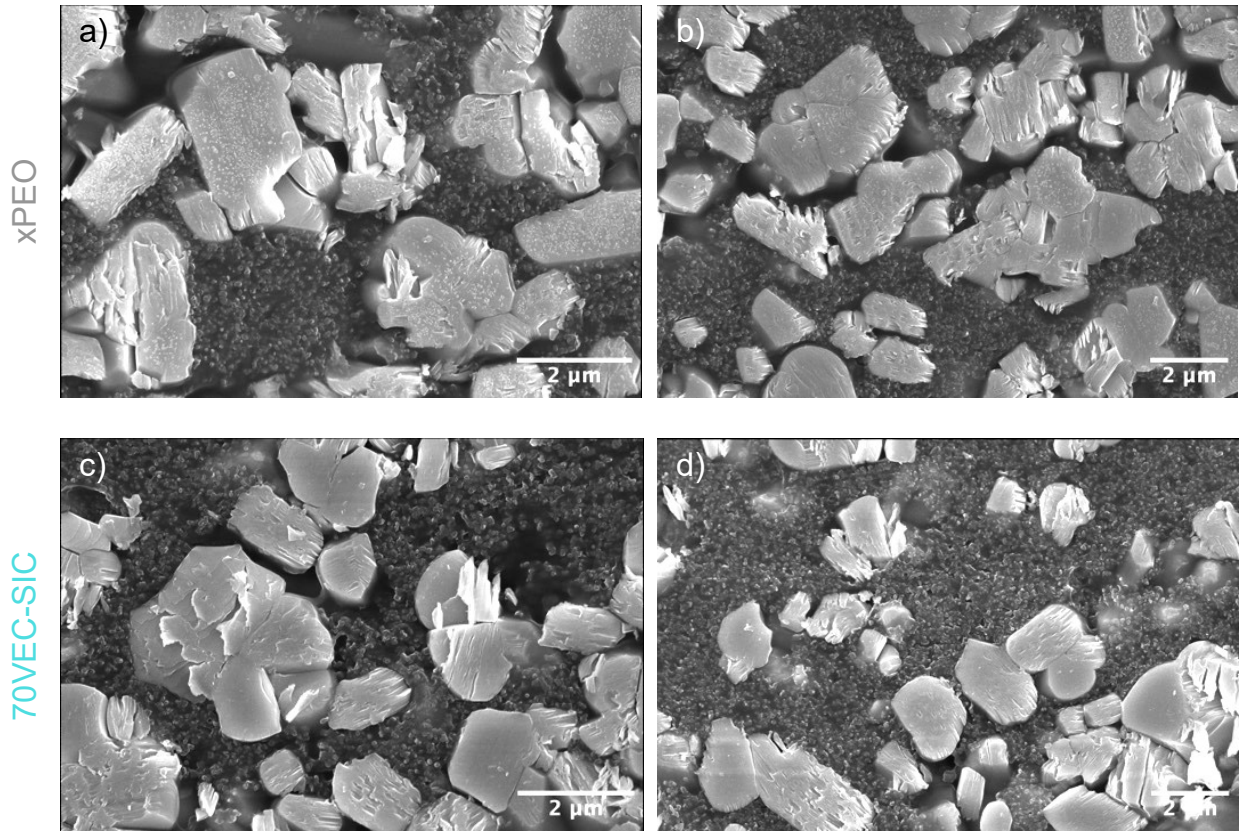

Figure S3. High magnification SEM images of the cross-section of the composite cathodes prepared via infiltration with (a, b) xPEO polymer electrolyte, and (c, d) 70VEC-SIC polymer electrolyte.

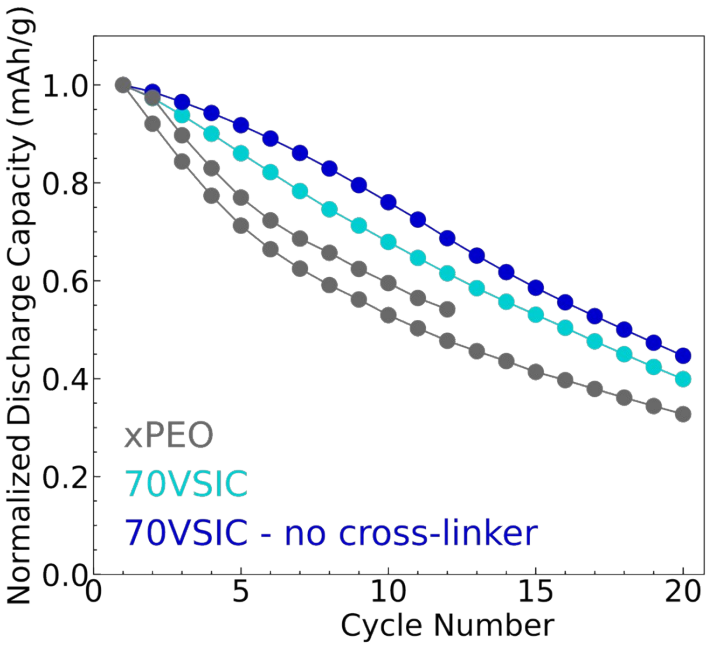

Figure S4. Discharge capacity normalized to the corresponding cell's 1st cycle discharge capacity. The two grey colored plots represent two repeat cells made for the xPEO PE.

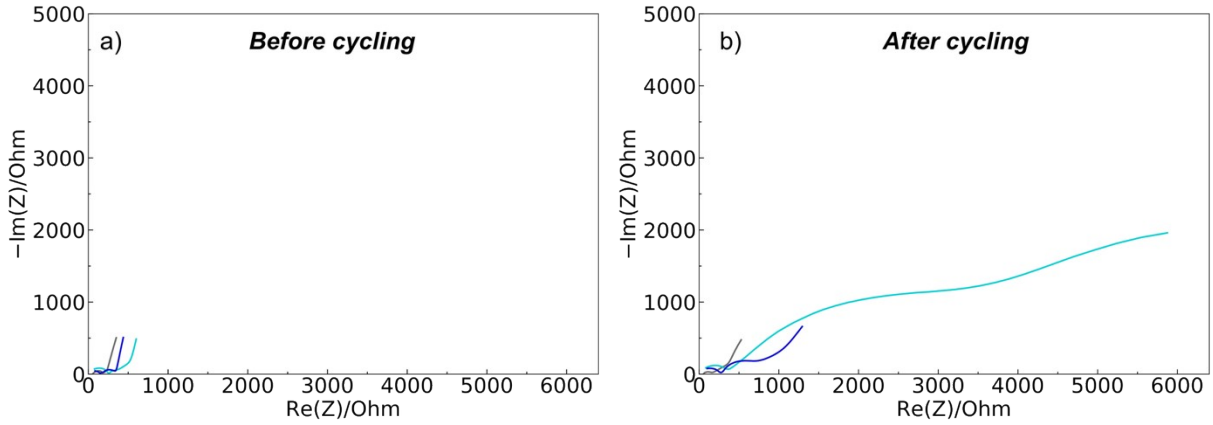

Figure S5. EIS Nyquist plots of the Li||NMC622 cells made with the three PE types (xPEO, 70VEC-SIC, 70VEC-SIC - no crosslinker), obtained (a) before cycling, and (b) after 20 cycles at 50 μA/cm^2, 70 °C, discharged to 2.9 V. Fitted circuit parameters and the various frequency ranges are listed in **Table S2**.

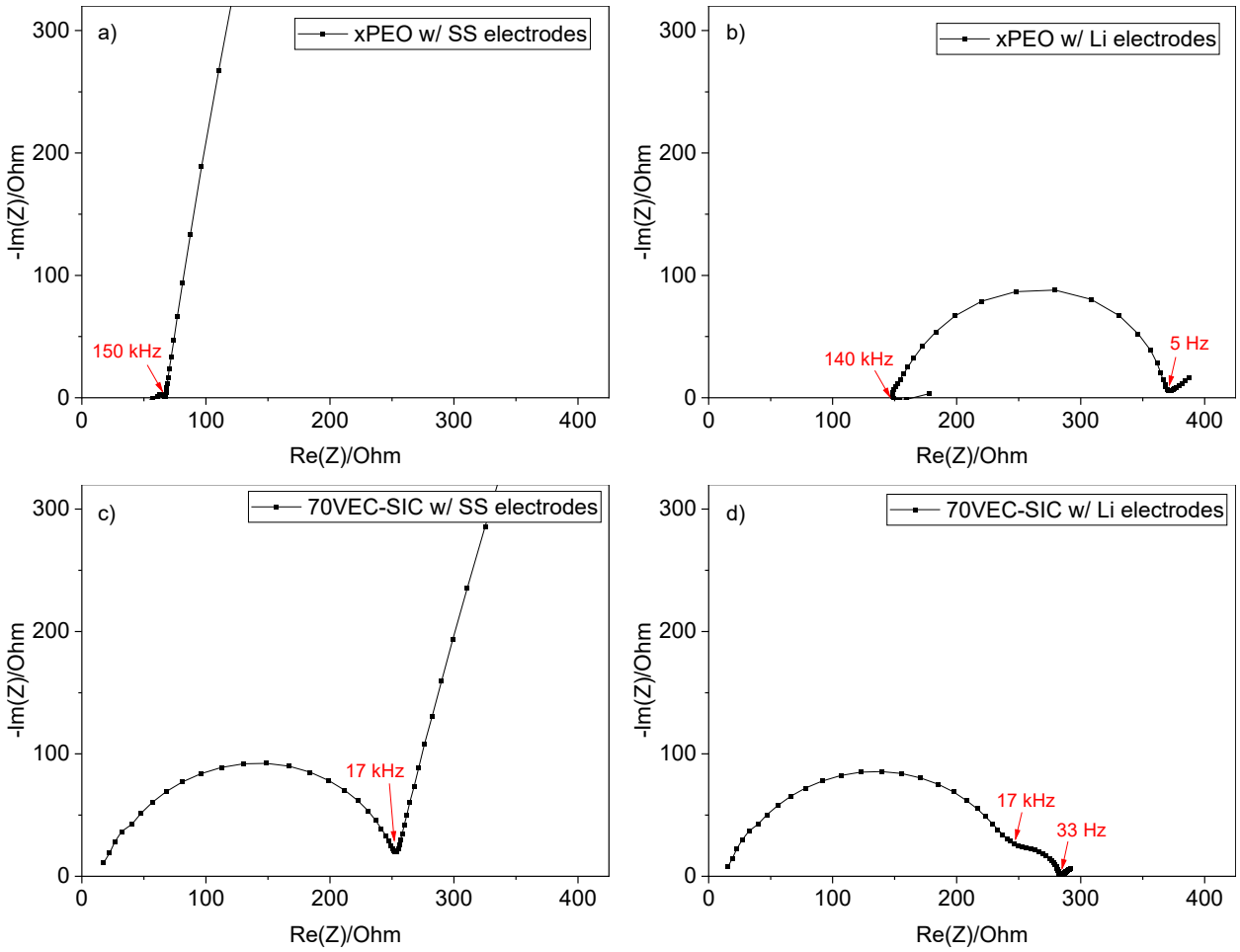

Figure S6. EIS Nyquist plots of the reference symmetric cells made with xPEO or 70VEC-SIC polymer electrolytes, utilizing either (a, c) stainless-steel (SS) blocking electrodes, or (b, d) Li metal non-blocking electrodes. These data were reported in our previous publications. [1-3]

Note S1

Electrochemical impedance spectroscopy (EIS) was conducted before and after 20 cycles. Cell impedance of all the cells grew after cycling (**Figure S5**). **Figure 4** presents breakdown analysis of the total cell impedance into its various components: 1) total bulk impedance of PE phase (separator + catholyte), observed in the high frequency range, 2) total impedance of the PE decomposition layers at the electrode interfaces (SEI_D + CEI_D), observed in the mid frequency range, 3) impedance of the rock-salt layer formed at the surface of cathode particles during cycling (CEI_{RS}), observed in the low frequency range, and 4) total interfacial impedance (total cell impedance minus total bulk impedance). The 'high', 'medium', and 'low' frequency ranges fell between > ~200 kHz – 6 kHz, ~6 kHz – 1 Hz, and < ~1 Hz, respectively, for these cells (**Table 2**). Reference symmetric cells of PEs made with either stainless-steel (SS) blocking electrodes, or Li metal non-blocking electrodes were utilized to aid in distinguishing the various spectral features (**Figure S6**).

We ascribe the observed SEI_D + CEI_D impedance growth primarily to the CEI_D, because the PE|Li interfacial impedance remained relatively unchanged for xPEO and 70VEC-SIC in Li||NMC and Li||Li cells, respectively, after multiple plating/stripping cycles (as reported in our previous works) [1-3].

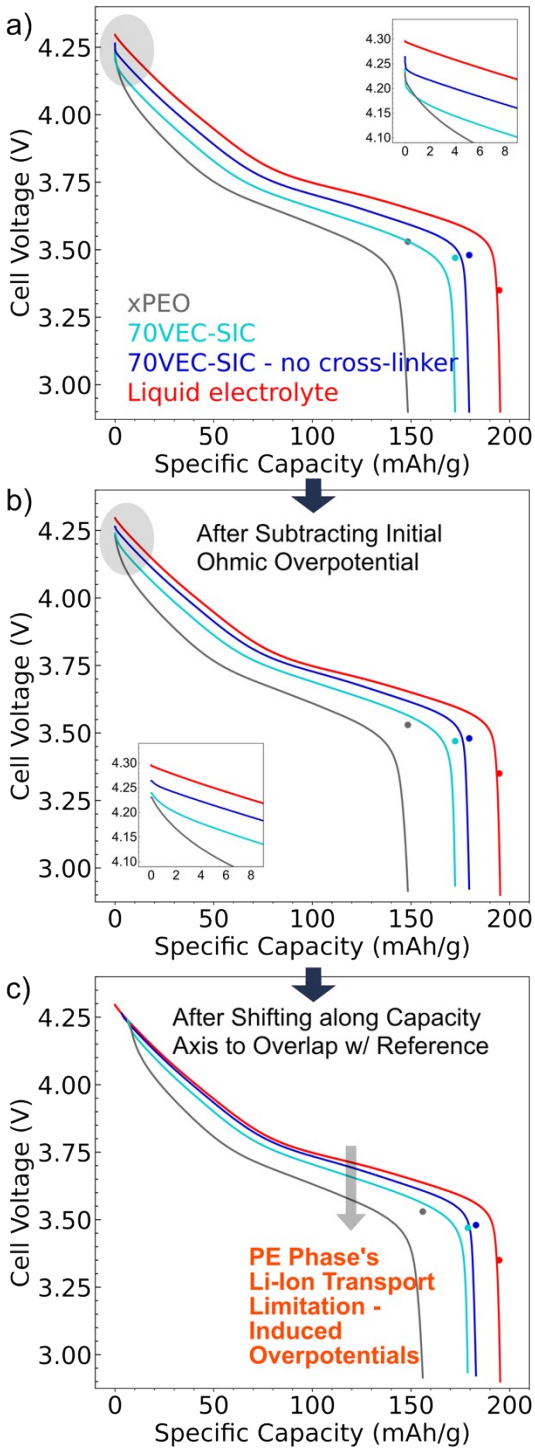

Figure S7. a) Unprocessed first-discharge voltage profiles of the three types of cells ('xPEO', '70VEC-SIC', '70VEC-SIC (no crosslinker)') cycled at 50 μA/cm^2, 70 °C. A comparison with a reference cell made with a liquid electrolyte and cycled @ ~C/100 is included to get a close to thermodynamic voltage profile. Circles correspond to the cells' OCV values obtained after 1-hour rest following the discharge.

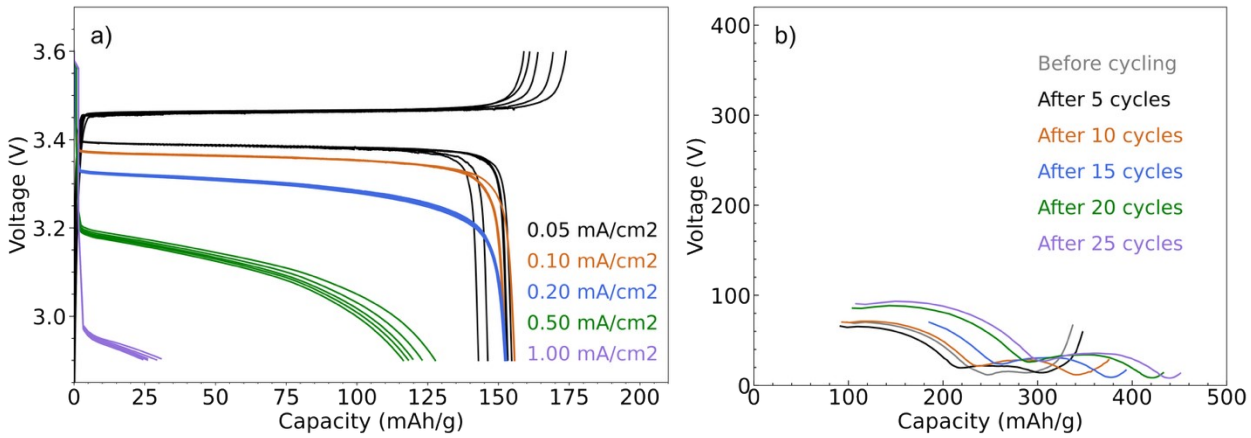

Figure S8. a) Charge/discharge voltage profiles of a Li||LFP cell made via the infiltration method using 70VEC-SIC PE. Five cycles were conducted at each current density. b) EIS of the cell in a) before cycling and after 5 cycles at each of the current densities, in discharged state.

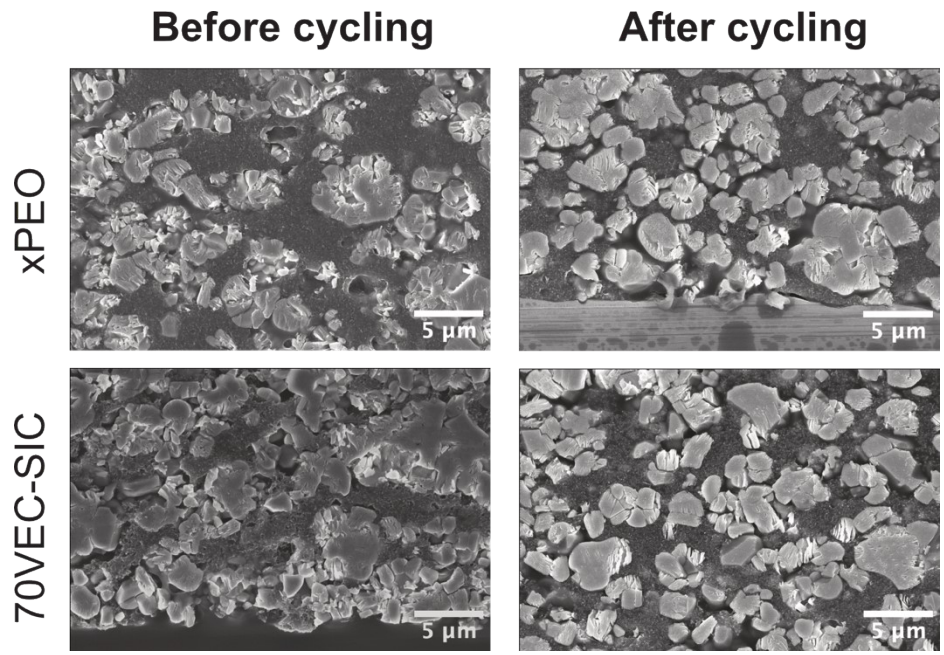

Figure S9. Cross-section SEM images of the uncycled and cycled cathodes made with xPEO or 70VEC-SIC PEs.

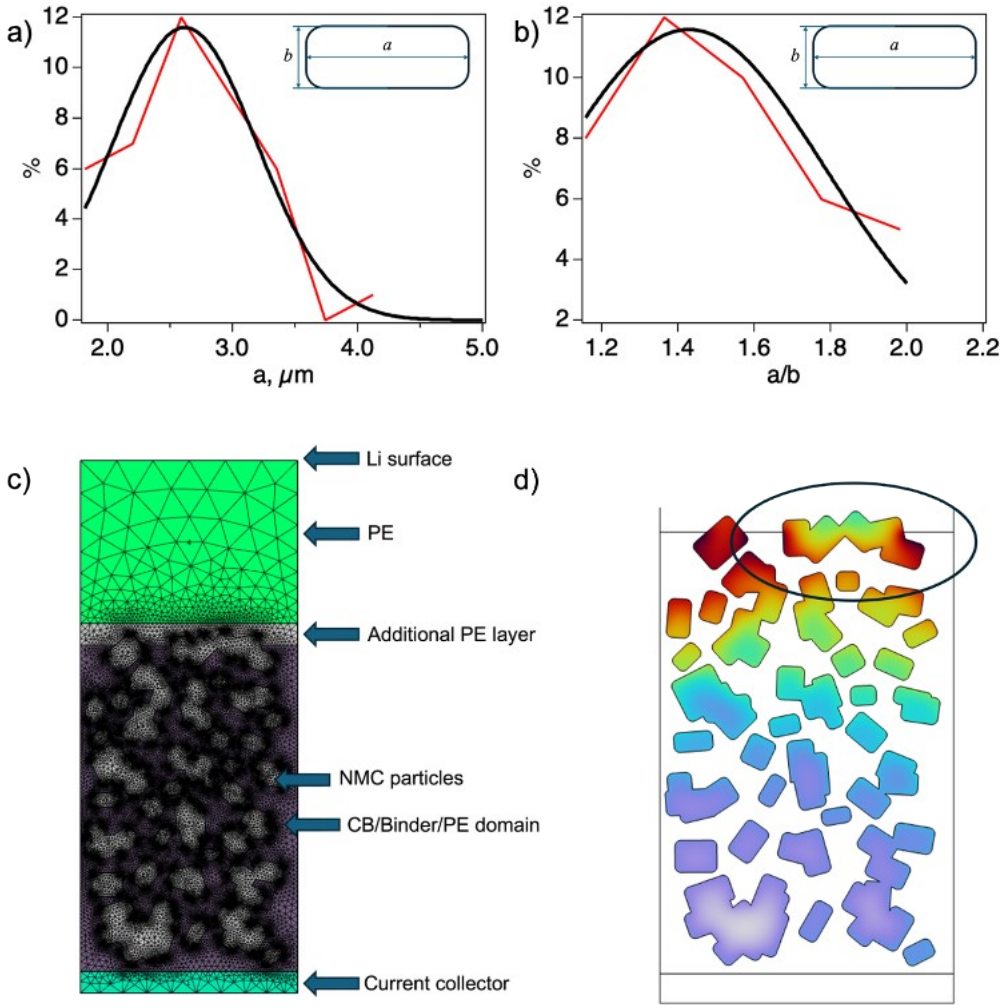

Figure S10. NMC622 particle size distribution in 2D as represented by rectangles with the long side (a), and the ratio of the sides (b). (c) Schematic of the cathode/electrolyte domain. (d) Incomplete delithiation of a large particle (circled) that is not completely covered by the CB/binder and contacts electronically insulative PE.

One separate simulation was performed with some of the large particles allowed to stick out of the binder and contact the PE. The particles that were left protruding out of the binder/electrolyte domain show the importance of the uniform binder coverage. Since the PE has very low electronic conductivity, the parts of the particles that are not covered with binder/CB have to rely on electron transport via NMC. If a particle is large this creates underutilized regions of NMC, even though they are the closest to the lithium electrode (**Figure S10d**).

References

[1] Sahore, R.; Armstrong, B. L.; Tang, X.; Liu, C.; Owensby, K.; Kalnaus, S.; Chen, X. C. Role of Scaffold Architecture and Excess Surface Polymer Layers in a 3D-Interconnected Ceramic/Polymer Composite Electrolyte. *Advanced Energy Materials* 2023, 13 (19), 2203663.

[2] Sahore, R.; Owensby, K. D.; Armstrong, B. L.; Ock, J.; Lehmann, M. L.; Ullman, A. M.; Kalnaus, S.; Chen, X. C. Pathway to High Rate Capability in Interconnected Composite Electrolytes: A Case Study with a Single-Ion-Conducting Polymer. *ACS Applied Energy Materials* 2024, 7 (24), 11714–11723.

[3] Owensby, K. D.; Ock, J.; Sahore, R.; Meyer, H. M., III; Self, E. C.; Lin, Y.-R.; Tsai, W.-Y.; Chen, X. C. The Impact of Lithium Anode Interface on Capacity Fade in Polymer Electrolyte-Based Solid-State Batteries. *ACS Applied Energy Materials* **2024**, *7* (22), 10271-10280.